 doi:10.20944/preprints202103.0079.v1

Article

On the wireless microwave sensing of bacterial membrane potential in microfluidic-actuated platforms

Marc Jofre [1,2,*], Lluís Jofre [3] and Luis Jofre-Roca [2]

[1] Department of Research and Innovation. Fundació Privada Hospital Asil de Granollers, Granollers 08402 (Barcelona), Spain.
[2] Department of Communications and Signal Processing, Universitat Politècnica de Catalunya - BarcelonaTech, Barcelona 08034, Spain.
[3] Department of Fluid Mechanics, Universitat Politècnica de Catalunya - BarcelonaTech, Barcelona 08019, Spain.
* Correspondence: marc.jofre@upc.edu

Abstract: The investigation of the electromagnetic properties of biological particles in microfluidic platforms may enable wireless monitoring and interaction with functional activity of microorganisms. Of high relevance is the membrane potential as it is one of the most important parameters of living cells. In particular, the complex mechanisms of the cell's membrane potential are comparable to the dynamics of bacteria membranes, providing a simplified platform for advancing the current techniques and knowledge of general bio-particle dynamics. In this work, we provide a theoretical analysis and experimental results on the microwave detection of bacteria on a microfluidic-based framework for sensing the membrane potential of bacteria. The results enable to further advance the state-of-the-art of electromagnetic bacteria sensing and microfluidic control, and their implication for measuring and interacting with the cell and its membrane potentials, which is of great importance for developing new biotechnological-engineered systems and solutions.

Keywords: Bacteria, elasto-inertial focusing, microfluidics, microwaves, membrane potential, sensing, shear stress, single cell detection, system-on-a-chip.

1. Introduction

Recent scientific and technological advancements are producing a plethora of interaction and sensing possibilities, eventually leading to communication that will drastically change the way we link with cells [1-2]. The continued efforts to satisfy more challenging sensing, interaction and processing requirements offer opportunities for disruptive technological advancements in science and engineering. One relevant example is the convergence of disciplines like micro, bio, information technologies and cognitive sciences. These technological advances have crystallized in different brands and concepts known and used in multiple research fields at present, such as Lab-on-a-chip (LoC) [3]. For example, improved miniaturized systems allowing the integration of a complete system on a chip (SoC) with sensing, processing and wireless interaction functions including microfluidic and microwave subsystems [4].

A main focus of the convergence of disciplines is in biological solutions and technologies involving interaction with cells. A cell is often thought of as the smallest unit of a living organism, made up of even smaller parts, each with its own functionality as shown in Figure 1. Cells can be categorized in eukaryote (e.g., mammalian cells, neurons) and prokaryote cells (e.g., bacteria). There are several differences between the two, but a major distinction between them is that eukaryotic cells have a distinct nucleus containing genetic material, while prokaryotic cells do not have a distinct nucleus and have free-floating genetic material instead. Besides this distinction, there are several similarities in the different elements that form these two types of cells, such as cell wall, cell membrane, cytoplasm, and ribosomes among others. Additionally, bacteria can be categorized according to gram-negative and gram-positive families (originally due to the permeability of specific dyes when observing them under the microscope), it mostly also relates to different

 doi:10.20944/preprints202103.0079.v1

membrane, or wall structure, as depicted in Figure 1. Generally, gram-negative bacteria have an outer membrane, which expresses itself by different responses of the bacteria, like for example virulence and antibiotic resistance.

Furthermore, recent microbiology advances have determined that bacteria are an easily characterizable model organism with an extraordinarily complicated set of abilities, comparable to the whole brain sensing [5-6]. Among them is quorum sensing, a cell-cell signaling system that may have a common evolutionary origin with eukaryotic cell-cell signaling, and related to action potentials. For example, the action potential in neurons (eukaryotic cells) is used to transmit information to other neurons, whilst equivalent action potentials are generated in bacterial biofilms to transmit information to external or other bacteria, in the surrounding. The two systems are behaviorally similar, but quorum sensing in bacteria is more easily studied in depth than cell-cell signaling in eukaryotes [7]. Because of this relative ease of study, bacterial dynamics are also more suited to direct interpretation than eukaryotic dynamics, i.e., those of the neurons [8].

An action potential is a rapid rise and subsequent fall in voltage, or membrane potential, across a cellular membrane with a characteristic pattern. A significantly important current intensity is required to initiate a voltage response in a cell membrane; if the current is insufficient to depolarize the membrane to the threshold level, an action potential will not be triggered [9-10]. Membrane potential refers to the difference in charge between the inside and outside of a cell (such as neurons or bacteria), which is created due to the unequal distribution of ions on both sides of the cell. The term action potential refers to the electrical signaling that occurs within neurons, or bacteria biofilms, arising from changes in membrane potential from ion concentrations in the vicinity of membranes. Hence, action potentials have some similarities to membrane potentials. In the case of action potentials, the electrical and chemical potential can be treated independently from each other. This is in contrast to membrane potentials as they can lead to chemical changes, and vice versa [11].

In this work, we focus mainly on sensing tasks as a way of monitoring and interacting with bacteria cells. Hence, it is important to note that an action potential's transmitted signal comes from a locally excited/generated membrane potential. In particular, for bacteria, but in some extent also in general for both prokaryotic and eukaryotic cells, membrane potentials are dynamic in time and in location, and related to a diverse number of tasks mainly grouped in energy (e.g., motility, ATP synthesis, membrane transport and antibiotic resistance) and signaling/processing (e.g., antibiotic resistance, communication, cell division and pH homeostasis) [11], which at the cell level may enable novel approaches for diagnosing and treating health diseases such as cancer [12-13].

In particular, the membrane potential, given a specific location, changes in time in response to a stimulus or perturbation as depicted in the bottom graph in Figure 1. The time response corresponds to an initial or stable resting potential (negative voltage value) which then, given a disruption, it produces a depolarization (the membrane becomes less negative in voltage), succeeded by a repolarization (the membrane potential returns to the voltage resting potential), followed by a hyperpolarization (increase in negative voltage of the membrane potential), to finally end at the stable resting voltage potential. All these processes occur over a few milliseconds and millivolt differences [7-8,11,14].

Preprints (www.preprints.org) | NOT PEER-REVIEWED | Posted: 2 March 2021 doi:10.20944/preprints202103.0079.v1

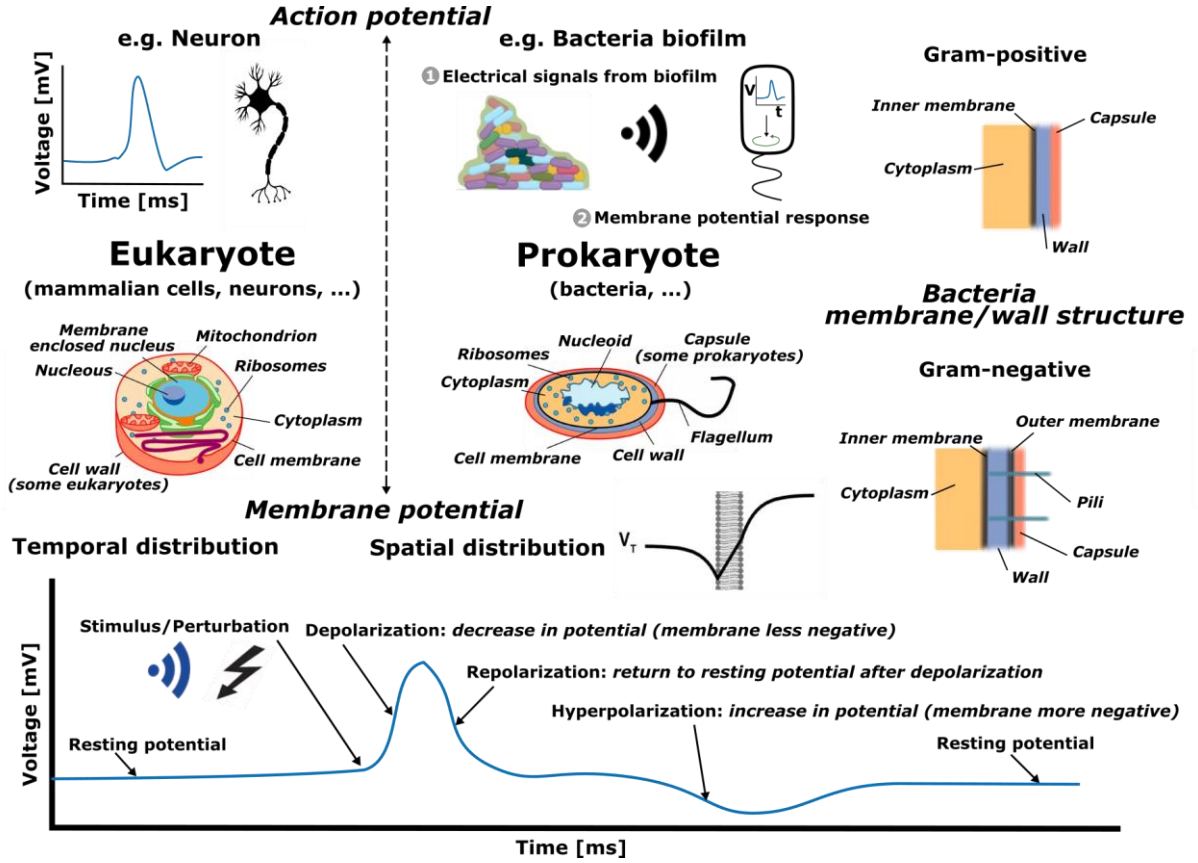

Figure 1. Cells are categorized in eukaryote (e.g., mammalian cells, neurons) and prokaryote cells (e.g., bacteria). Additionally, bacteria are categorized according to gram-negative and gram-positive, relating to different membrane or wall structure as depicted in the up-per/middle-right panel of the figure. The dynamic process known as action potential happens in both types of cells. In particular, the membrane potential, given a specific location, changes in time in response to a stimulus or perturbation as depicted in the bottom graph.

We have introduced the basics of membrane potentials that are critical for microbiological investigations. However, in-depth analyses and concepts of membrane potential are beyond the scope of this article; a vast review can be found in [7-8,11,14].

Bacterial membrane potentials are different from neural potentials because of the size of bacteria and their membrane structure. Hence, different techniques have been developed and utilized to measure bacterial membrane potential quantitatively and temporally. Gold standard methods for membrane potential sensing are patch clamping and voltage, or fluorescent, sensitive dyes [11]. In patch clamping, one measures the absolute value of the membrane potential. On the contrary, with voltage sensitive dyes, one can only monitor changes in the membrane potential. Both methods are effective but invasive and laborious. Instead, electromagnetic approaches can be applied to cells suspended in solutions [15-18].

Electro-magnetic (EM) wave biosensors are attracting a lot of attention due to multiple benefits, such as being minimally invasive and cost effective [19-21]. Recent advances in microwave sensing [22-23], together with other applications of microwaves in the GHz frequencies [24-26], enable to explore new narrow band windows for membrane interactions research. Studies of the effects of a weak (non-thermal) microwave radiation on the cellular structures have clearly shown that the reaction of cells to weak microwave radiation is highly selective in frequency. In particular, the reaction of cells becomes extremely strong at certain frequencies. Although various researchers have reported different values of the resonant frequencies obtained in experiments, all these frequencies were in the range of GHz [14,27]. Furthermore, microwave frequencies allow monitoring inside the human body, with considerable penetration (cm) distance and resolution (mm) [28].

Preprints (www.preprints.org) | NOT PEER-REVIEWED | Posted: 2 March 2021 doi:10.20944/preprints202103.0079.v1

To approach this monitoring, microfluidics has been proven a useful technology for interacting and controlling microorganism's functions through the interplay with fluid streams [29]; performing these functions without mechanical moving parts, and with little noise generation in the process. In particular, inertial and elasto-inertial microfluidics, using Newtonian and non-Newtonian fluids, respectively, can provide efficient single-particle flows in the center of a microfluidic channel and cell focusing that guarantees optimal sensitivity and accuracy [30-36]. In addition, microfluidics is a resourceful platform for the administration of perturbations to bacteria [37-39] that can trigger the generation of membrane potentials as a means, for example, of self-protection [11].

2. Detection techniques

It is of relevant importance to detect bacteria individually in order to monitor and interact with their membrane potential on a one-by-one basis. Furthermore, individually detecting and analyzing microorganisms is of capital importance in a variety of fields encompassing health, industry and environment, for applications ranging from diagnosis in clinics, pharma manufacturing, beverages production and solid fuel-treatment deposits [40-41], among others.

In this work, not all the possibilities for detecting bacteria are listed, but only a representative portion regarding physical measuring methods in order to show the general characteristics. Therefore, it is compared several elements of relevance, in single-cell bacteria physical methods sensing, to show the general trade-offs encountered. Extensive and broad revisions of scientific measurement techniques can be found in [19,42-44]. In this work, it will not be described, or compared, molecular techniques, such as PCR, microarrays, ELISA or others like culture methods, respirometry, fluorometers and bioluminescence, to mention a few; a detailed discussion can be found in [41,45-47].

Parameters of interest for detecting bacteria include: specificity, sensitivity, limit-of-detection, and time-to-result. In detail, specificity is the capacity of a detection technique to discern or detect only the relevant microorganisms or their characteristics of interest. However, specificity is largely dependent on many factors. In particular, it is strongly influenced by chemical reagents or dyes. Instead, in this work we compare the capacity of the physical measurement technique to focus on measuring a specific parameter (parameter specificity) of the microorganism that is meant to be detected, imprinted in the specific physical change that is sensed. In this regard, sensitivity is used in general to quantify the capability of a detection system to capture minimum signals from microorganisms of interest. In the practical side, it is more interesting the limit-of-detection, but it is dependent on many additional factors, like for example bacteria strains. Nevertheless, it is not the aim of this work to compare the sensitivities or limits-of-detection between different detection techniques, but to compare their sensing capabilities. Hence, the term sensing volume is used in order to apply a common quantifiable parameter among the detection techniques, and allowing a fair comparison between them. The sensing volume here refers to the minimum volume actually sensed in the procedure used for the detection in the different techniques, and quantified in liters. Another parameter of interest is the time-to-result, which accounts for sample preparation, incubation (if needed) and measurement process; for some techniques, or depending on the sample size, it can take a long time and is also a function of many factors that need consideration. Instead, in order to compare different techniques, we have taken the specific time to obtain the physical measurement part of the technique, and normalize it to the time taken to measure an equivalent $100\mu L$ of sample, which is a common analysis volume for most applications to gather sufficient statistics (determined by Poissonian distribution of particulates in the detection processes) for the concentrations of interest. Therefore, the measurement time indicated does not take into account incubation processes or other preparation steps.

In Figure 2, it is shown the comparison of several reported detection techniques in the literature based on the measurement time, in minutes, and the sensing volume, in liters. The values reported for the sensing volume correspond to either the geometrical dimension of the sensing volume or the actual indicated liquid volume. If multiple values were

Preprints (www.preprints.org) | NOT PEER-REVIEWED | Posted: 2 March 2021 doi:10.20944/preprints202103.0079.v1

reported in the same study, the better value (i.e., best performance) is reflected in the chart. The reported experiments were performed with bacteria or particles with similar size to allow for a better comparison in the chart.

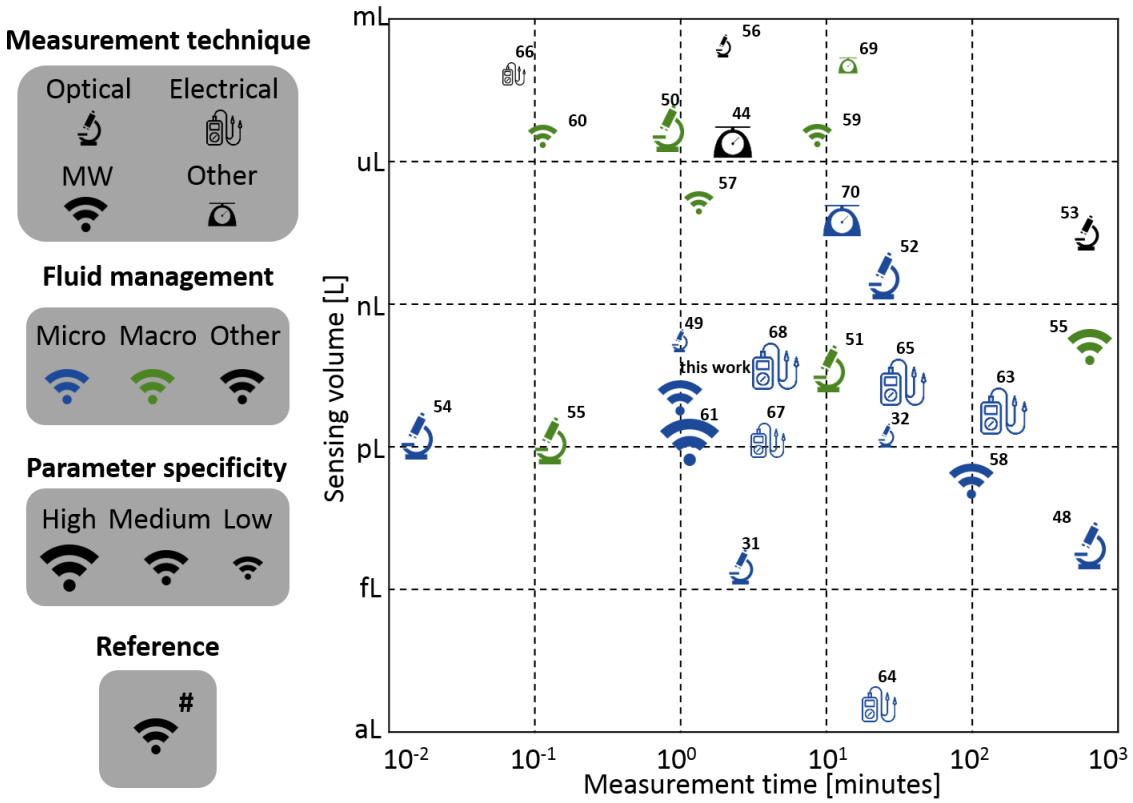

Figure 2. Comparison of several reported physical based methods for bio-particle detection techniques in the literature (optical, microwave, electric and some others). In order to compare the different measurement times reported for different total analyzed volumes, this time has been normalized to the equivalent time to analyze a final total volume of 100μL. Fluid management is divided in micro, macro and other. Finally, the parameter specificity is divided in high, medium and low. A trend between the measurement time and the sensing volume is encountered, since in order to have more sensibility (smaller volumes sensed) more time is needed in order to measure a large part of the sample.

The measurement techniques are grouped in four categories: optical, microwave, electric and others. Optical techniques refer to measurement systems where both the microorganism illumination and sensing is performed using light-based techniques [31-32,48-56]. Microwave systems make use of electromagnetic illumination and detection at higher frequencies in the order of GHz ($> 1\,GHz$ and $< 1\,THz$), where the equivalent wavelength is similar or smaller than the fundamental characteristic dimension of the measurement system [this work,57-62]. Electrical techniques consist mainly of approaches that make use of low frequency electrical signals ($< 1\,GHz$) for measurement, where the equivalent wavelength is larger than the fundamental characteristic dimension of the measured system [63-68]. Other techniques consist of different physical-based (e.g., mass spectroscopy, magnetic detection) measurement systems that have been proposed or exist for detecting bacteria [44,69-70].

In terms of fluid management, defined as the relevant fluid mechanics principles that govern the system, it is divided into three categories: micro, macro and other. Micro refers to managing fluids in flow channels with cross-section dimensions smaller than $100\mu m$. Macro refers to flows handled in fluidic channels or containers with at least one cross-section dimension larger than $100\mu m$. Other fluid-controlled techniques refer mainly to systems in which there is no intentional fluid flow management to make the particles flow through the sensing area.

Preprints (www.preprints.org) | NOT PEER-REVIEWED | Posted: 2 March 2021 doi:10.20944/preprints202103.0079.v1

Finally, the parameter specificity is divided in three levels: high, medium and low. The parameter specificity is defined for measurement techniques that aim at sensing a particular physical property of the particulates, rather than just detecting the whole element only. The high level refers to experiments which have used a labeling technique or the physical measurement extracts high-level information from the bacteria. The medium level refers to studies where the physical measurement extracts qualitative information with little direct relation to the bacteria's biological state or characteristics. The low level refers to studies that only detect bacteria without any further insight. Figure 2 shows a common trade-off between measurement time and sensing volume. This is expected since (roughly) in order to have more sensibility (smaller volumes sensed) more time is needed to measure a large part of the sample. Furthermore, there is an important gap in the literature with respect to having small sensing volumes and using microwave techniques.

There is no specific technique that reins in all regions but it is true that over the past 30 to 40 years many advances have been performed in optical [31-32,48-56] and low/medium-frequency electrical techniques [15,63-68,71-73]. In contrast, this work is based on microwave techniques at the microfluidic scale, falling therefore in the center of the chart both in terms of sensibility and measurement time, which is of interest for bacteria detection applications, and especially relevant for sensing and interacting with bacterial membrane potentials.

3. Microfluidic elasto-inertial focusing of particles

Over the past decade, microfluidic technology has been proven essential in biological research to precisely control the motion and position of microorganisms in a fluid flow, and is consequently the methodology selected in this work to complement the microwave-based sensing techniques to achieve hydrodynamic focusing of microorganisms. In this regard, inertial focusing [74] is an effective technique for controlling particle (particles are utilized as a surrogate of biological species) positions in microfluidic devices at moderate Reynolds numbers (Re), i.e., $Re \sim 1 - 100$; in fluid mechanics [75], Re characterizes the ratio of inertial to viscous forces used to classify flow regimes as laminar (flow organized in layers) or turbulent (flow dominated by velocity fluctuations). As first studied in [76] for Newtonian fluids, in a cylindrical pipe, initially randomly distributed particles are known to focus to an annulus located between the center and wall of the pipe, while in square-section channels, following the symmetry of the system, particles instead focus to four equilibrium regions centered at the faces of the flow-bounding walls [77]. However, when utilizing viscoelastic fluids, i.e., a type of non-Newtonian material that exhibits both viscous and elastic behavior when undergoing deformation, particles have been found to migrate toward the centerline of pipes/channels in the case of fluids with constant viscosity [78]. The underlying principle of these phenomena is the balance of the hydrodynamic forces acting on the particles while advected by the flow. Particularly, in the case of elasto-inertial microfluidic systems [32], four main forces need to be considered: (i) wall-interaction force, (ii) shear-gradient lift force, (iii) viscoelastic force, and (iv) Stokes' drag force.

3.1. Elasto-inertial forces in microfluidic flows

The wall-interaction force becomes important in the vicinity of solid boundaries, where the streamlines of the flow are diverted toward the side of the particle away from the wall, accelerating the fluid, causing a lower pressure on the centerline-side of the particle, and resulting in the wall-interaction force depicted in Figure 3, responsible for separating the particle from the wall. Moreover, in microfluidic devices, due to the moderate Reynolds numbers encountered, fluids flow following a parabolic velocity profile, i.e., laminar regime, generated by shear stresses induced by the wall. Consequently, as represented in Figure 3, particles experience a larger relative velocity on the side away from the centerline of the pipe/channel. This velocity dissimilarity causes pressure differences that impart a force directed toward the wall, and referred to as shear-gradient lift force. As a result, in the case of Newtonian fluids, the location where these two forces balance each other determines the equilibrium position of particles in the wall-normal direction of the flow.

Preprints (www.preprints.org) | NOT PEER-REVIEWED | Posted: 2 March 2021 doi:10.20944/preprints202103.0079.v1

However, when particles are submerged in nonhomogeneous shear flows, i.e., viscoelastic fluid, an additional viscoelastic force is generated on the particles in the direction of decreasing shear rate [79], which modifies the inertial equilibrium position by forcing particles to migrate toward the centerline of the pipe/channel. Finally, as included in Figure 3, Stokes' drag is the frictional force that particles experience in a uniform flow and proportional to the velocity difference between particles and a viscous fluid. In the case of long, straight pipes/channels, viz. with no curvature, Stokes' drag force is responsible for accelerating/decelerating particles until they achieve the same velocity as the flow. This last force, however, does not play a direct role in determining the steady-state position of particles in the wall-normal directions as it acts, mainly, in the streamwise direction of the flow.

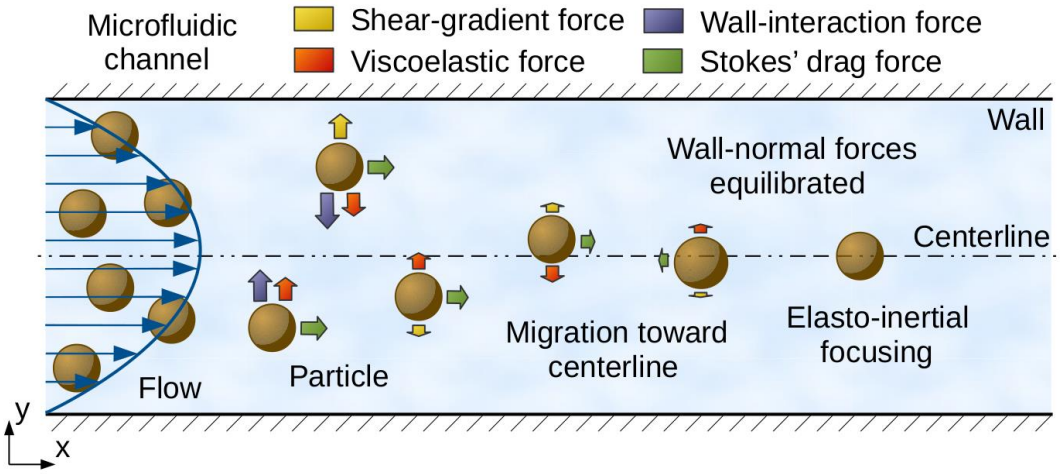

Figure 3. Schematic of the hydrodynamic forces acting on particles in an elasto-inertial microfluidic channel. The particles are randomly distributed at the inlet of the channel. The interaction, and final balance, of the wall-normal forces results in the focusing of the particles at the centerline. The main forces are: shear-gradient lift force (yellow), wall-interaction force (violet), viscoelastic force (red), and Stokes' drag force (green).

3.2. Dimensionless numbers and characteristic regimes

The characterization of elasto-inertial fluid motion and particle focusing in wall-bounded microfluidic flows is efficiently assessed by considering the Reynolds number defined as $Re = \frac{\rho_f U_c D_h}{\mu_f}$, where ρ_f and μ_f are the density and dynamic zero-shear viscosity of the fluid, U_c is the centerline fluid velocity, and $D_h = 2WH/(W+H)$ is the hydraulic diameter with $W$and H the width and height of the microfluidic channel, respectively, and the Weissenberg number, characterizing the ratio between elastic and viscous forces, given by $Wi = \tau_f \dot{\gamma} = \frac{\tau_f U_c}{D_h}$, where τ_f is the fluid relaxation time, and $\dot{\gamma} = 2Q/(HW^2)$ is the characteristic shear rate with $Q = WHU_m$ the volumetric flow rate and $U_m = (2/3)U_c$ the mean fluid velocity in a laminar channel flow. The ratio between these two dimensionless numbers corresponds to the elasticity number $El = Wi/Re = \tau_f \mu_f/(\rho_f {D_h}^2)$, which only depends on the channel dimensions and fluid properties. Other parameters that are of second-order importance include the geometry of the channel, the strength of the shear-thinning effect, the initial position of particles, and the blockage ratio defined as $\kappa = d/D_h$ with d the particle diameter; when $\kappa < 0.25$, blocking effects can be assumed to be negligible.

As studied in [79], the equilibrium position for most particles in a viscoelastic fluid is either at $Y_p \equiv y_p/D_h > \approx 0.15$ or at the channel axis, where Y_p is the normalized vertical position away from the centerline. This is due to the occurrence of the inertial-force peak at $Y_p \approx 0.15$, which is explained in the lines below. For a second-order fluid, the viscoelastic force on a particle is $F_{VE} = \frac{-40}{3}\pi \rho_f {U_c}^2 \kappa d^2 El\, Y_p$, with the negative sign indicating that the force drives the

Preprints (www.preprints.org) | NOT PEER-REVIEWED | Posted: 2 March 2021 doi:10.20944/preprints202103.0079.v1

particle toward the center of the channel, in contrast to the shear-gradient lift force, which causes the particle to migrate away from the central axis, given by [30] $F_{SG} = C_{SG}\rho_f {U_c}^2 \kappa d^2$ for $Y_p \approx< 0.3$, where C_{SG} is the shear-gradient lift coefficient, which is a positive function of Y_p and has a maximum value of $C_{SG} \approx 0.05$at $Y_p \approx 0.15$, and is equal to zero at both $Y_p = 0$ and $Y_p \approx 0.3$; the wall-interaction force $F_{WI} = -C_{WI}\rho_f {U_c}^2 d^6/{D_h}^4$ (C_{WI} is the wall-interaction lift coefficient) is not considered in this analysis because it is assumed that the particle is close to the centerline and sufficiently away from the wall. The relative magnitude between F_{VE} and F_{SG} determines whether the particle can be focused at the centerline or not. In fluid flows with $El \gg 1$, the viscoelastic force overcomes the maximum shear-gradient inertial force and the particle migrates toward the centerline. In contrast, for fluid flows with $El \ll 1$, the particle stops at a location before F_{SG}reaches its maximum. Therefore, the balance between F_{VE} and F_{SG} at $Y_p \approx 0.15$ leads to an estimate for the critical elasticity number of $El_c \approx 0.025 \sim 0.01$.

The channel length L required for particles to achieve equilibrium positions at the centerline, i.e., particle focusing, is based upon the magnitudes of the forces described above and their variation along a particular channel. As an extremely important design parameter, this length must be estimated carefully. Following a scaling analysis for straight channels, in [30] it was estimated the focusing length L_F based on the transversal particle migration velocity U_p [80], which was calculated using the balance of F_{SG} and Stokes' drag force, defined as $F_D = 3\pi\mu_f d U_p$, obtaining the expression $L_F = \frac{3\pi\mu_f {D_h}^2}{C_{SG}\rho_f U_c d^2} \sim \frac{\pi\mu_f {D_h}^2}{C_{SG}\rho_f U_c d^2}$, where C_{SG} takes values in the range $0.02 - 0.05$, F_{VE} is zero at the channel centerline and is consequently not considered to estimate L_F. In the case of significantly small particle Reynolds numbers, i.e., $Re_p = Re(d/D_h)^2 \ll 1$, the focusing mechanisms may be degraded due to the diffusion rate of particles becoming comparable to the inertial migration velocities [81]. This limitation is evaluated by means of an equivalent particle Peclet number defined as $Pe_p = \frac{U_p L_c}{D} = \frac{C_{SG}{\mu_f}^2 D_h {Re_p}^2}{2k_B T\rho_f}$, where $L_c = D_h/2$ is a characteristic length scale, and $D = k_B T/3\pi\mu_f d$ is the Stokes-Einstein diffusion coefficient of a particle with k_B the Boltzmann constant and T the temperature of the system. For the diffusion effects to be negligible in inertial microfluidic systems, it is required that $Pe_p \gg 1$.

In addition to the inertial and viscoelastic forces creating equilibrium positions for particles within the cross section of a channel, particles suspended in a fluid will interact in a flow with finite inertia to create particle trains with regular spacing in the streamwise direction of the flow. This phenomenon has been observed, for example, in millimeter-scale pipe flows [82] and rectangular microchannels [83]. Therefore, particle concentration is also a critical factor affecting the focusing behavior and accuracy. Aside from the potential interparticle interactions, there are wake effects due to particles being concentrated in a few relatively narrow streamlines. In order to identify when these effects become important, the number of particle diameters per channel length, or length fraction, $\lambda_{mf} = d/L$ is defined, which is more appropriate than a volume fraction given that particles are focused to single streams. One can convert from a volume fraction α to λ_{mf} using the relation $\lambda_{mf} = \frac{6HW\alpha}{\pi d^2}$. For $\lambda_{mf} \gg 1$, focusing to a single stream is not to be expected due to wake interactions between particles, whereas the opposite is true for $\lambda_{mf} \ll 1$. Note that for a given α, λ_{mf} increases quadratically with decreasing d, such that accurate focusing of smaller particles requires significantly more (quadratically) diluted solutions.

3.3. Microfluidic design for microwave-based sensing of bacteria

Elasto-inertial microfluidics can be prepared by additives comprising biological, or synthetic, polymeric powders. For example, $500ppm$ of polyethylene oxide (PEO) polymer in a phosphate-buffered saline (PBS) solution can be used to force particles to focus into a single-stream at the center of a microfluidic channel [31]. As explained above, elasto-

Preprints (www.preprints.org) | NOT PEER-REVIEWED | Posted: 2 March 2021 doi:10.20944/preprints202103.0079.v1

inertial focusing is achieved under specific conditions which depend mainly on the Reynolds and Weissenberg numbers and, to a second-order approximation, on the blockage ratio and length fraction. The interplay between these different parameters is visually summarized on the regime diagram depicted in Figure 4. The vertical critical-Reynolds-number ($Re_c \approx 2300$) line separates the laminar flow region, where the balance between forces discussed in this section applies, from the transitional/turbulent region not typically considered in microfluidic applications due to the complexities introduced by the increased velocity fluctuations. In parallel, the diagonal critical-Elasticity-number ($El_c \sim 0.01$) line delineates the separation between elasto-inertial and inertial focusing regimes. The red dashed rectangle indicates the parameter design space, which is detailed below, targeted for sensing bacteria using microwave-based detection techniques.

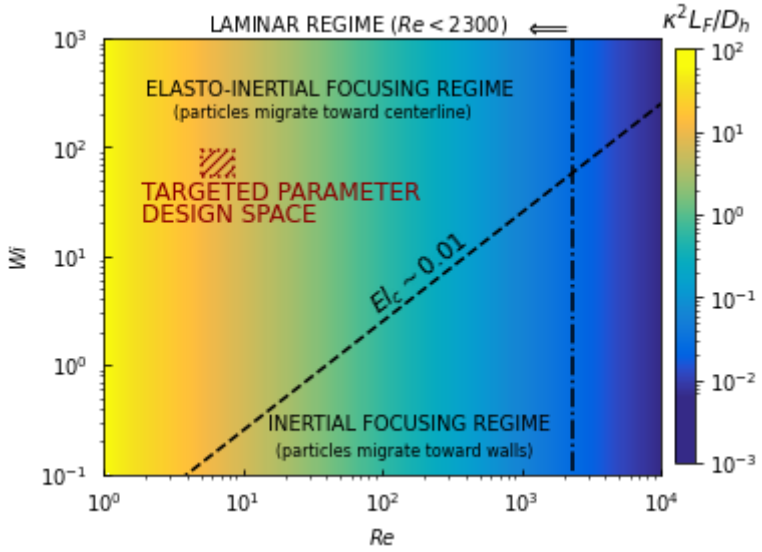

Figure 4. Regime diagram of the dimensionless Reynolds (Re) and Weissenberg (Wi) numbers for viscoelastic fluids of inertial flows in microfluidic channels. The colormap corresponds to the squared blockage ratio (κ) multiplied by the slenderness ratio (L_F/D_h); a value of $C_{SG} = 0.05$ has been utilized. The diagonal dashed line (critical elasticity number $El_c \sim 0.01$) separates elasto-inertial from inertial focusing regimes, while the vertical dot-dashed line separates laminar ($Re < 2300$) from transitional/turbulent flow regimes. The red dashed rectangle indicates the parameter design space targeted for sensing bacteria using microwave-based techniques.

The constraints of the microfluidic channel designed are imposed by manufacturing, sensing, fluid properties, and biological limitations, and correspond to: (i) the width, height and length of the channel are $W = H = 50\mu m$ and $L = 60mm$ as standardized by manufactured microchips; (ii) the average fluid velocity provided by the pressure pump is tuned to $U_m = 0.2$m/s (the range $U_m = [0.17 - 0.225]$ m/s is considered to calculate the targeted parameter design space) to provide sufficient exposure time (approximately $250\mu s$) for sensing the biological species on a field-of-view of $50\mu m$ as typically required by a microscope; (iii) the viscoelastic fluid utilized is based on a solution of water with $500ppm$ of $0.4\,MDa$ PEO solution and resulting in $\rho_f = 1000Kg/m^3$kg/m^3, $\mu_f = 1.95mPa \cdot s$ and $\tau_f = 11.39ms$ [28]; and (iv) the diameter of the bacteria considered is $d \sim 1\mu m$ with a reasonable particle number density for preparing solutions in the order of $n_p \sim 5 \cdot 10^4\, particles/mL$. This set of values results in the elasto-inertial microfluidic design located within the red dashed rectangle depicted in Figure 4, and corresponding to $Re \approx 8$ which is smaller than 2300 (laminar regime), $Wi \approx 68$ which is larger than 1 (viscoelastic fluid), $El \approx 9$ which is larger than $El_c \sim 0.01$ (elasto-inertial focusing regime), $Pe_c \approx 11$ which is sufficiently larger than 1 (inertial regime), $\kappa = 0.02$ which is smaller than 0.25 (blocking effects are negligible), $Q = 30\mu L/min$, $\lambda_{mf} \sim 1.25 \cdot 10^{-4}$ which is much smaller than 1 (dilute

Preprints (www.preprints.org) | NOT PEER-REVIEWED | Posted: 2 March 2021 doi:10.20944/preprints202103.0079.v1

solution), and $L_F \sim 1m$ (a value of $C_{SG} = 0.05$ has been utilized) which is more than an order of magnitude larger than $L = 60mm$.

The inadequacy of the design in terms of focusing length, i.e., $L_F \sim 1 \gg L = 0.06m$, is expected due to the small diameter of the particles considered; elasto-inertial manipulation of particles is typically limited to $Re_p \gg 0.1$ as L_F scales inversely with d^2. A solution recently proposed to overcome this challenge is based on oscillatory microfluidics [81]. Unlike traditional steady-flow microfluidics, oscillatory microfluidics switches the streamwise direction of the flow at a low frequency. Due to the symmetry of the velocity field along the flow axis, the elastic and inertial forces acting on the particles preserve their directionality when the flow is switched, and consequently, by exploiting this symmetry, the focusing length can be extended indefinitely, even though the channel itself has a much shorter, fixed length. Based on the dimensionless numbers described above, the frequency of the oscillations f_{mf} and the corresponding distances traveled by the particles can be defined for a given system. In particular, f_{mf} is limited in the lower end by the distance L the particles can travel within the microchip. On the higher end, f_{mf} is limited by the entrance length, viz. streamwise distance required for the flow to develop. In the case of laminar flow, this upper limit is quantified by the dimensionless Womersley number, which expresses the pulsatile flow frequency in relation to viscous effects, defined as $Wo = D_h\sqrt{\frac{2\pi f_{mf}\rho_f}{\mu_f}}$.

Small Womersley numbers, i.e., $Wo < 1$, indicate that the flow is fully developed for most of the oscillation period, and consequently entrance-length effects can be ignored. In general, the wall-normal particle focusing positions achieved by this oscillatory flow method are the same as for traditional steady-flow systems [84]. Particularly for the microfluidic design considered in this work, selecting an oscillation frequency based on the mean velocity of the fluid and a length equal to the channel length, i.e., $f_{mf} = U_m/L$, the Womersley number obtained is $Wo = 0.16 < 1$, which is sufficiently small for entrance-length effects to not impact the elasto-inertial focusing of particles.

4. Microwave detection

In many situations, electromagnetic waves interact with inhomogeneous particles and the corresponding electromagnetic-matter interaction process is referred to as scattering. In this work, we will center the analysis on this phenomenon to monitor biological particles dynamics rather than using detection effects as commonly used. A general scheme of the configuration of electromagnetic illumination and detection of scattering by a small particle (e.g., bacteria or polystyrene beads) in a liquid medium (e.g., water) is depicted in Figure 5. One of the goals in scattering experiments is to infer information about the relative permittivity, or refractive index, of the particle from measurements on the scattered field. Here, particle refers to a region in space characterized by a dielectric complex permittivity (ϵ_s, σ_s) which is different from that of the surrounding medium (ϵ_m, σ_m).

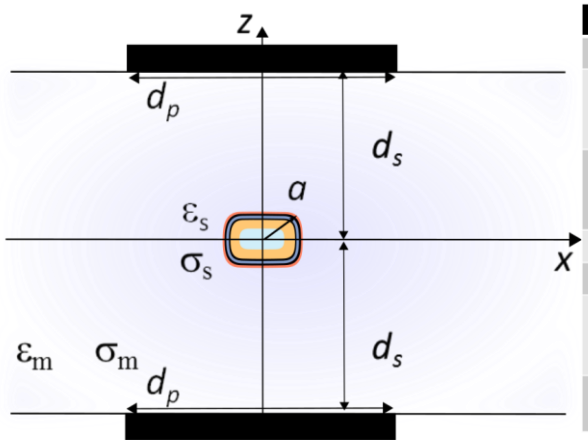

	ε_r @ few GHz	σ [S/m] @ few GHz	Thickness/Volume
Bacteria	74	0.17	0.2-2μm (~1μm³)
Membrane (two membranes for gram-negative)	10	$5{\cdot}10^{-8}$	7nm
Wall	60	0.73	200nm (gram-negative) / 300nm (gram positive)
Ribosomes	-	-	10nm-20nm
Nucleoid	80	0.15	~0.5μm³
Cytoplasm	67	0.20	~1μm³ (half of the volume is occupied by the nucleoid)
Capsule (mostly on gram-negative)	15	$3{\cdot}10^{-6}$	200-300nm

Preprints (www.preprints.org) | NOT PEER-REVIEWED | Posted: 2 March 2021 doi:10.20944/preprints202103.0079.v1

(a) **(b)**

Figure 5. The electromagnetic response of bacteria depends on their shape and size, their internal structure, and the electric conductivity and permittivity of the different bacterial cell components, which may depend on the bacterial physiological state. (a) Scheme of the configuration and relevant values depicted, where ϵ_s stands for permittivity of the cell, σ_s conductivity, a radius, ϵ_m permittivity of the medium, σ_m conductivity, d_p is the length of the illumination and detection plates and d_s distance to the cell (considered equally spaced). (b) Conductivity, permittivity and thickness/volume of the different parts of bacteria have been extracted from [85-86] and congruent with [58,63].

In particular, at microwave frequencies, and for the typical dimensions of the experimental setups, the conditions of scattering are of near-field (in contrast, for light frequencies where the conditions are of far-field). Furthermore, since the particle is isolated due to using dilute enough solutions (normal samples of interest), it is only considered single scattering (not considering multiple scattering) as described in [87-89].

4.1. Scattering by a small spherical particle

When an electromagnetic wave impinges on an object, the incident wave can be modeled as a uniform electromagnetic wave (sufficiently accurate since the emitter is much larger than the particle); assuming (i) the electromagnetic wave to be polarized in the z direction and (ii) the particle to be a small spherical region of radius a with permittivity ϵ_s. Essentially, the particle sees a constant field as the plane wave impinges on it (and almost electrostatic field on the incident field). The incident field polarizes the particle making it resemble an electric dipole. Since the incident field is time-harmonic, the small electric dipole will oscillate and radiate like a Hertzian dipole in the far field, but it can also be analyzed in the near-field. A Hertzian dipole can be approximated by a small current source so that $\vec{J}(\vec{r}) = \hat{z} I l \delta(\vec{r})$. The vector potential $\vec{A}$ due to a Hertzian dipole is $\vec{A}(\vec{r}) = \frac{\mu}{4\pi} \iiint d\vec{r'} \frac{\vec{J}(\vec{r'})}{|\vec{r}-\vec{r'}|} e^{-j\beta|r-r'|} = \hat{z} \frac{\mu I l}{4\pi r} e^{-j\beta r}$, where μ is the permeability, I is the time harmonic current, l is the length of the dipole, r is the distance from the particle and β is the complex wavenumber.

4.1.1. Near-Field regime

The electric field is given by $\vec{E} = -j\omega\vec{A} - \nabla\Phi$, where the scalar potential term dominates over the vector potential in the near field of the scatterer. The scalar potential $\vec{\Phi}(\vec{r})$ is obtained from the Lorenz gauge as $\nabla \cdot \vec{A} = -j\omega\mu\epsilon\Phi$, and resulting in $\Phi(\vec{r}) = \frac{-1}{j\omega\mu\epsilon} \nabla \cdot \vec{A} = \frac{-Il}{j\omega\epsilon 4\pi} \frac{\partial}{\partial z} \frac{1}{r} e^{-j\beta r}$. When close to the dipole, by assuming that $\beta r \ll 1$, a quasi-static approximation can be utilized for the potential (equivalent to ignoring retardation effects) $\frac{\partial}{\partial z} \frac{1}{r} e^{-j\beta r} \approx \frac{-cos\theta}{r^2}$, and reducing the potential to $\Phi(\vec{r}) \approx \frac{ql}{4\pi\epsilon r^2} cos\,\theta$. The dipole induced by the small particle is formed in response to the incident field. The incident field can be approximated by a constant local static electric field $\vec{E}_{inc} = \hat{z}\, E_i$. The corresponding electrostatic potential for the incident field is then $\Phi_{inc} = -\hat{z}\, E_i$, so that $\vec{E}_{inc} \approx -\nabla\Phi_{inc} = \hat{z} E_i$. The scattered dipole potential from the spherical particle in the vicinity of it and in the same axis of illumination is given by $\Phi_{sca} = E_s \frac{a^3}{r^2}$. The electrostatic boundary problem is $E_s = \frac{\epsilon_s - \epsilon}{\epsilon_s + 2\epsilon} E_i$. As a result, the electric scattered near-field is given by $\vec{E}_{sca} = \left[\frac{k^2 a^3}{r} \frac{\epsilon_s - \epsilon}{\epsilon_s + 2\epsilon} - \frac{a^3}{r^3} \frac{\epsilon_s - \epsilon}{\epsilon_s + 2\epsilon}\right] E_i\, \hat{z} \approx -\frac{a^3}{r^3} \frac{\epsilon_s - \epsilon}{\epsilon_s + 2\epsilon} E_i\, \hat{z}$. A similar derivation can be obtained for the magnetic scattered near-field given by $\vec{H}_{sca} \approx \frac{k\, a^3}{r^2} \frac{\epsilon_s - \epsilon}{\epsilon_s + 2\epsilon} H_i\, \hat{z}$ [90], where $\vec{H}_{inc} = \hat{z}\, H_i$ is the incident magnetic field.

Preprints (www.preprints.org) | NOT PEER-REVIEWED | Posted: 2 March 2021 doi:10.20944/preprints202103.0079.v1

4.2. Microwave scattering of bio-particles

In microwave standards [91-92], $10^2\ W/m^2$ is a typical magnitude of radiation fluxes below which thermal effects are negligible, which is approximately four orders of magnitude larger than the minimum microwave intensity levels at which the spontaneous excitation of membranes was observed in experiments [9,11,19,85-86,93-97]. For instance, in this work, the calculations are estimated assuming illumination of $100\ mW$ during $500\ ms$ at $25\mu m$ distance, which yields an irradiance of around $1.7 \cdot 10^2\ W/m^2$ when averaged. This estimation is close to the non-thermal regime in a $30\mu m\ x\ 30\mu m$ effective field of view on a $1\mu m$ particle.

In Figure 6, measured experimental values of bacteria permittivity and conductivity in the frequency range $1 - 10\ GHz$ are shown using the technique described in [98-99]. These measured values, although for a bacteria culture sample they are indicative for single-bacteria measurement, are relevant for deriving the expected detected scattering levels for $1\mu m$-size particles representative of bacteria.

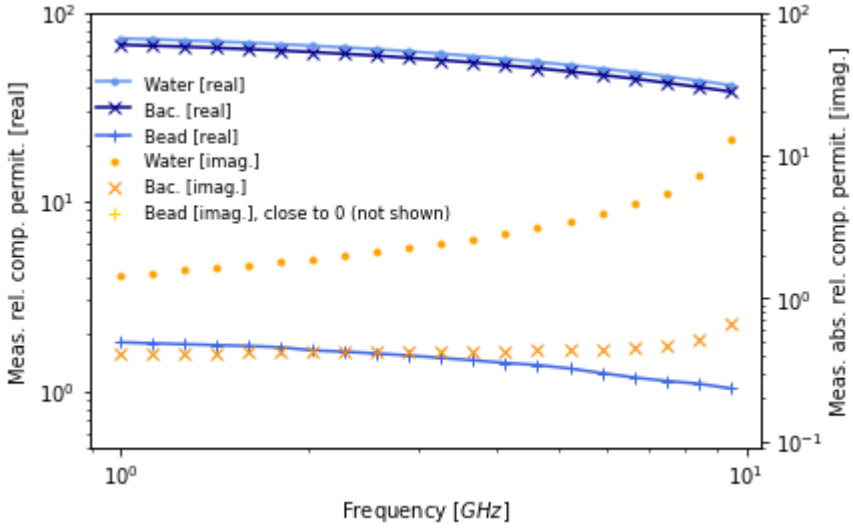

Figure 6. Microwave complex permittivities for small $1\mu m$ particles. Measured complex permittivity of bacteria in the range $1 - 10\ GHz$ using the technique described in [98-99], which are in concordance with [58].

The complex permittivity of polystyrene beads differs substantially from the permittivity of the medium (water), resulting in a better scattering detectability. However, the permittivity of cells at rest, or when generating a potential, do not differ much from its medium. As a result, cells are almost transparent at microwave frequencies compared to the medium in which they are submerged; a similar scenario is encountered at optical frequencies. The membrane's capacitance (related to the real part of the complex permittivity) of bacteria depends on its surface area, while the conductivity of the membrane depends on its cross-sectional area [11,100]. Hence, it is not expected to easily observe a large variation between a cell at rest and generating an action potential, because these physical dimensions are not expected to change significantly. Moreover, the expected complex permittivity, shown in Figure 7 (a), and scattering signal for a bacteria in an action potential state, depicted in Figure 7 (b), where a 1% change has been assumed to show the difficulty of achieving detection discrimination with respect to bacteria at rest. In particular, in Figure 7 (a), the peak at $10GHz$ of the imaginary part of water and bacteria corresponds to a resonance due to intermolecular hydrogen bonding [101].

Preprints (www.preprints.org) | NOT PEER-REVIEWED | Posted: 2 March 2021 doi:10.20944/preprints202103.0079.v1

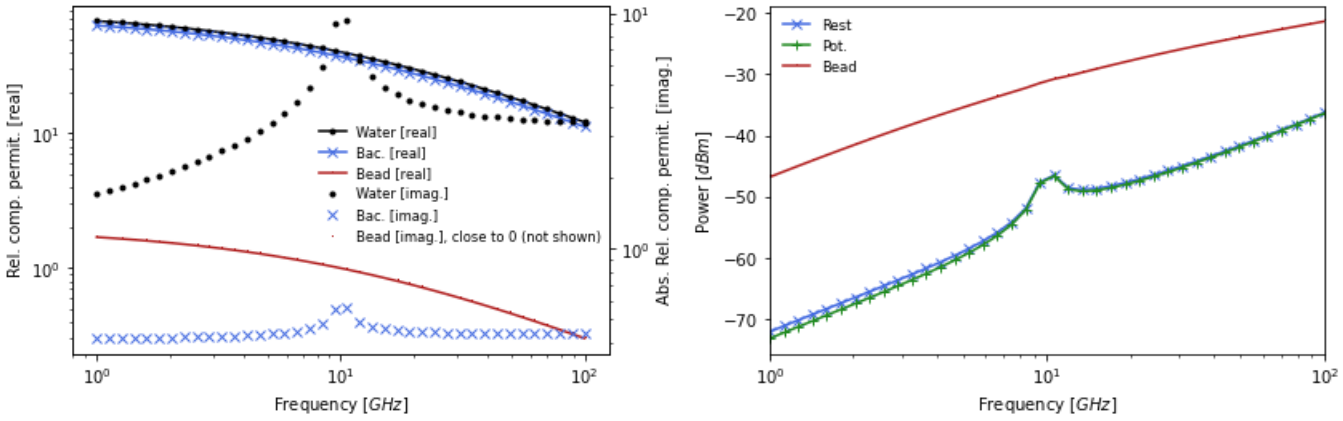

(a) **(b)**

Figure 7. Microwave complex permittivities and expected scattering signal levels (near-field) for small $1\mu m$ particles. (a) Complex permittivity values for the frequency range $1-100\ GHz$ approximated from [58,63,85-86], also adding water, bacteria in an action potential process and polystyrene beads. (b) Calculated expected scattering detection signal levels in power.

The required sensitivity for detection is shown in Figure 7 (b) in terms of power, in order to assess the required performance of the involved instrumentation for measuring these magnitudes. The required sensitivities might be achieved either by using novel detection instrumentation at microwave frequencies [102], or enhancing the response using cavity-like configurations [103-104]. In the following section, a framework for measuring the action potential is presented.

5. Membrane potential detection

Cellular, as well as intracellular, membranes exhibit a distinct nonlinear electrical behavior, due to the potential barrier resulting from the difference between the inner and outer electrolytes and the action of ion-pumps [105]. In the absence of an applied electromagnetic field, the transmembrane potential difference Δ_ϕ is equal to the cell resting potential V_0 ($\approx -100mV$ for a typical cell). When a low frequency field is applied, a transmembrane excess potential appears $\Delta_\phi = V_0 + \delta_\phi$. As a result, a transmembrane current density $\vec{J}_m$ is generated. The current-voltage response is known to be fairly well approximated by a nonlinear diode-like relationship of the form $J_m = J_0(e^{\delta_\phi/V_T} - 1)$ with typical values $J_0 \approx 10^{-5}A/cm^2$, $V_T \approx 5mV$ [104-110], where all electrical variables of interest (e.g., field, currents) may be derived from a single scalar potential $\Phi(\vec{r})$.

At optical frequencies, the use of a generated second harmonic to sense the action potential variation has been demonstrated by making use of the nonlinear susceptibility tensor [111-112]. In this work, we propose to sense the membrane's action potential at microwave frequencies by leveraging the non-linear behaviour of the voltage-current relationship of the membrane potential, as exploited in frequency mixing in radio- and microwave frequencies, which are mainly based on diodes [113]. Ideally, the charges respond to the rapid microwave wavelength as indicated in [14]. As shown in Figure 8 (b), the cell's membrane is illuminated with a microwave field, while the membrane's voltage working point in the non-linear voltage-current model will be determined by the cell's self potential state, as shown in Figure 8 (a). Depending on the state of the membrane potential, the scattered signals will have multiple generated frequency harmonics (due to the non-linear voltage-current model of the membrane), compared to the incident illuminating signal. In particular, using a Taylor series expansion for the first two terms of the transmembrane current density J_m, the expected efficiency of the second-order process at $\delta_\phi = 100\ mV$, compared to $\delta_\phi = 0\ mV$, is $2 \cdot 10^8$ times larger, while the second-order process at $\delta_\phi = 100\ mV$ compared to the first-order one is $3 \cdot 10^{-5}$, which is still significantly efficient [114].

Preprints (www.preprints.org) | NOT PEER-REVIEWED | Posted: 2 March 2021 doi:10.20944/preprints202103.0079.v1

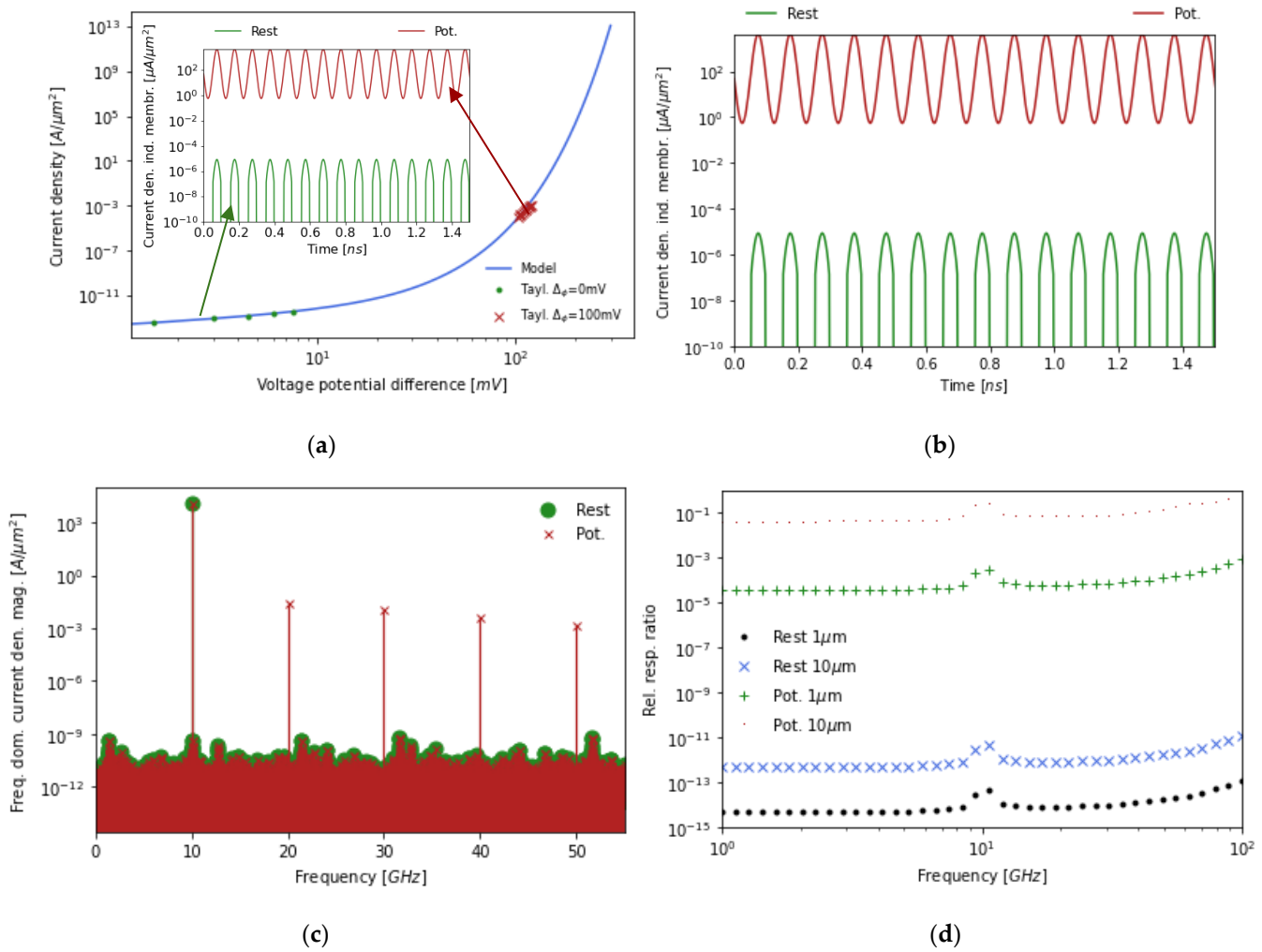

Figure 8. Nonlinear voltage-current response of the membrane potential. (a) Current density non-linear dependence with the differential voltage potential. (b) Induced current density due to an impinging microwave field at two different membrane potential states, while at rest and while at generating an action potential. (c) Frequency domain analysis where the fundamental frequency (pump) scattering due to the membrane, making it very difficult to sense the difference between the bacteria at rest and in an action potential state. Instead, the difference in the second frequency harmonic is around 8 orders of magnitude. (d) Frequency plot of the expected relative second harmonic responses at rest and at action potential state. Furthermore, the size of the bacteria scales the response with the cube of the radius.

Figure 8 (c) shows the nonlinear voltage-current response of the membrane potential responsible for generating harmonic frequencies. When impinging with a microwave frequency field (e.g., 10 GHz), an induced current density is generated on the working point of the membrane potential state, where its magnitude and frequency harmonics are incremented when the cell is at an action potential compared to a rest state. The fundamental frequency (pump) scattering due to the membrane (around $10nm$) is obscured compared to the scattering generated by the cell's bulk body (which is at least two orders of magnitude larger), making it very difficult to sense the difference between the bacteria at rest and in an action potential state. Instead, the second frequency harmonic, for instance, is characterized by a difference that is approximately 8 orders of magnitude between the two states. The reason for this result is that the frequency mixing is essentially sensing directly the effect of the membrane potential and not the whole bacterial body. The expected relative second-order response at different frequencies, with respect to the fundamental pump

Preprints (www.preprints.org) | NOT PEER-REVIEWED | Posted: 2 March 2021 doi:10.20944/preprints202103.0079.v1

frequency at rest and at action potential state, are shown in Figure 8 (d). As a note, the size of the bacteria scales the response with the cube of the radius, hence it is more challenging to detect $1\mu m$ than $10\mu m$ cells.

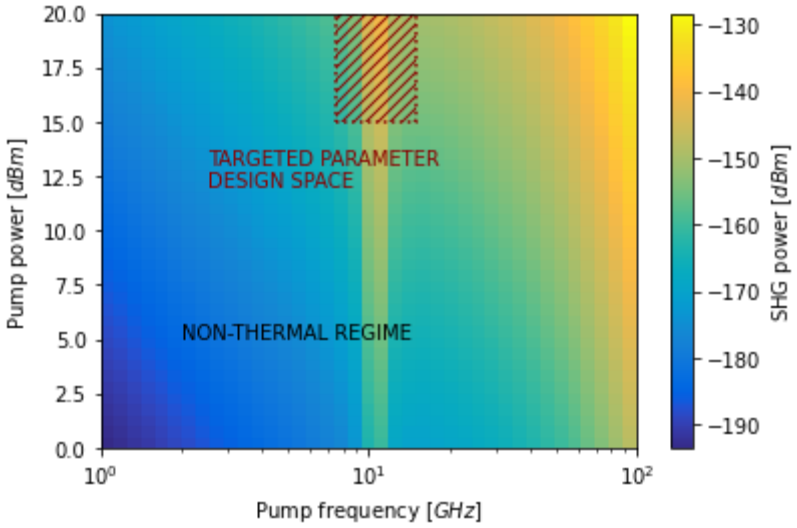

Figure 9. Second harmonic signal power dependence with pump frequency vs. pump power level. It is common for frequency conversion, the non-linear dependence of the power for the generated signal, while the dependence on frequency smoother.

Figure 9 shows the second harmonic signal level expected with respect to the pump frequency in the GHz range, and the pump power proposed to apply being in the mW range within the non-thermal regime. It is shown, as it is common for frequency conversion, the non-linear relation between pump power and generated harmonic's power.

For typical room temperature values and a bandwidth of $10Hz$, the noise level is around $-164dBm$, while at $4K$ cryogenic-temperature levels the equivalent noise is around $-182dBm$. Moreover, in the reactive near-field region of electromagnetic fields, the response levels of the electric and magnetic fields are not the same. In particular, the magnetic field, more closely related to currents, for higher frequencies computes to have a higher level of electromagnetic response, as shown in Figure 10. Nevertheless, the expected intensity levels and the equivalent noise levels are of the same order. A cryogenic low noise amplifier, or other similar techniques, may be appropriate to experiment with to detect such low signal levels to achieve a reasonable SNR and enter into the sensitivity limits of detectors. Further discussion is needed in this topic. As a first experimental approximation, it would be appropriate to use a very low-noise amplifier [115-116]. An additional option would be to use advanced quantum microwave-based techniques [102,117] to detect such low levels.

Preprints (www.preprints.org) | NOT PEER-REVIEWED | Posted: 2 March 2021 doi:10.20944/preprints202103.0079.v1

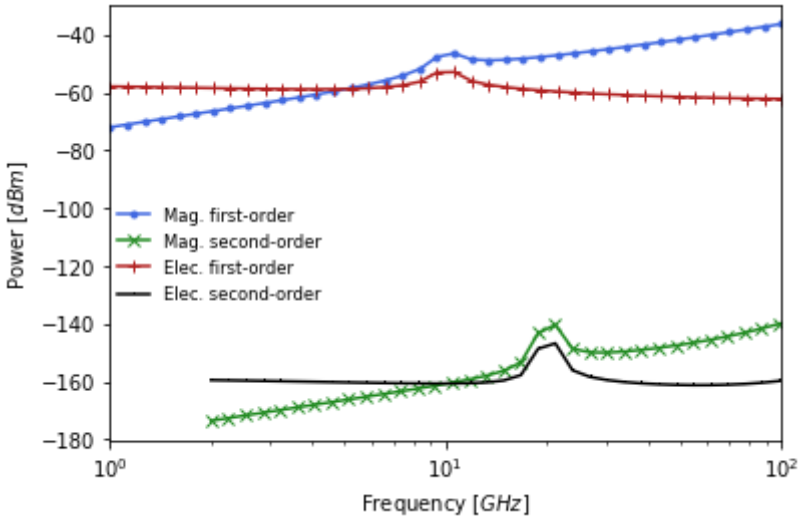

Figure 10. The signal levels regarding magnetic fields are slightly higher compared to electric fields for higher frequencies. Considering the magnetic or electric field, the second-order signal level is close to the noise level. Different techniques can be applied in order to improve the sensitivity of detectors, such as novel quantum electromagnetic sensing schemes.

As shown in Figure 10, it is relevant to explore the microwave $1-100\,GHz$ frequency range to inspect for resonances and enhance the detectability of such weak level signals. Other potentially expected resonances, shown in Figure 11, due to membrane potentials have been proposed [14], which may vary depending on the membrane thickness and other factors, but it is reasonably feasible that some will occur in the microwave range.

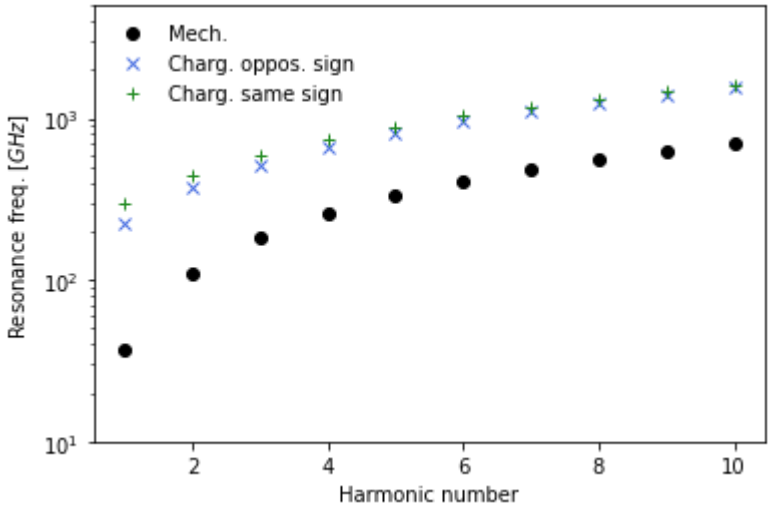

Figure 11. The speed of sound in water is around $1500m/s$ and the typical bacterial membrane thickness is in the order of $10nm$. Hence, mechanical resonances due to the shape and length of bacteria or due to movements of the membrane charges (either same sign or difference sign charges) have been proposed to exist and to have pronounced resonant characteristics in the microwave range.

Hence, the relevance of this work is also related to the potential of providing a method for further investigating these subtle sources of information encoded in the exploratory resonances resulting from mechanical disturbances, or due to electrical charges of same or opposite sign of bio-particles. In general, in this work, plain equations have been indicated both for the electric and magnetic fields in the near-field regime to deal with scattered fields from small bio-

Preprints (www.preprints.org) | NOT PEER-REVIEWED | Posted: 2 March 2021 doi:10.20944/preprints202103.0079.v1

particles. In particular, it has been derived that in order to wirelessly detect bio-particles, it is required a moderate level of sensitivity, around $-60dBm$, which is achievable with laboratory equipment. In the contrast, in order to monitor signals related to biological functionalities of the bio-particles, much better sensitivities are required, in the order of $-160dBm$, together with using derived scattering approaches different from monitoring the first order response. Because first order scattering approaches are fundamentaly related only to the physical dimensions of the bio-particles, while hig-order scattering signals are more related to intrinsic physical states of the biological particles.

6. Conclusions

Recent observations of the signaling roles of the membrane potential of bacteria has drawn the attention of researchers to study the dynamics of membrane potentials, many of which remain unexplored. Most membrane and action potential studies have focused on mammalian systems (eukaryote), which has led to a fundamental framework and models of cellular dynamics. As discussed in this work, the prokaryote realm (e.g., bacteria), however, is different for several important reasons, and hence the basic assumptions made by existing models may need careful consideration when applied to bacteria. Therefore, acquiring experimental measurements of bacterial membrane potential dynamics is essential to advance our understanding of how to apply these models.

The ability to manipulate biological cells is critical in a diversity of biomedical and industrial applications. In this regard, microfluidics-based cell focusing is an extremely useful functional operation preceding downstream biological analysis, since it allows the accurate wall-normal positioning of cells advected through microfluidic channels, and thus enables sophisticated cell manipulations in a passive manner. Furthermore, oscillatory inertial microfluidics achieves inertial particle manipulation and focusing in a previously inaccessible flow regime, which facilitates the introduction of controlled disruptions to bacteria through, for example, membrane-lysis processes in the form of shear stresses, compressive loads, and friction forces. This latter feature is especially useful in membrane potential analysis of cells and suggests the development of a microwave-fluidic platform for sensing and interacting in the short term.

In this work, we have summarized the general concepts of bacteria's membrane potentials. Furthermore, we have revised several detection techniques for bacteria together with a comparison between most of the relevant features among them. A microfluidic framework has been defined and quantified with operating regimes and specific values. Next, we have discussed the detection of bacteria using scattering microwave techniques, and measurements of complex permittivity have been presented for the analysis. Finally, we have proposed a method for enhancing and particularizing the membrane potential dynamics in the microwave range.

Eventually, an approach capable of observing electromagnetic changes in the activation region when disrupting membrane potential signals has been described. It is concluded that the sensitivities needed to detect the membrane potential of bacteria in the frequency range $1-100\,GHz$ impose the use of state-of-the-art microwave technologies, together with the potential existence of detection windows at frequencies around and above $10GHz$.

Fortunately, the requirements of microfluidics and microwave-based techniques converge to the need of miniaturization for sensitivity. However, microwave-microfluidic sensing and interaction with cells is still a largely uncharted territory in microbiology. We look further to apply this combined approach that holds the promise of facilitating new scientific discoveries in the areas of cell action and membrane potentials, and will ultimately help advance the status of controlling and sensing technologies.

Author Contributions: All authors contributed equally towards the conceptualization, preparation and validation of the manuscript.

Funding: This work was financially supported by the Beatriz Galindo Program (Distinguished Researcher, BGP18/00026), CICYT PID2019-107885GB-C31/REI/10.13039/501100011033 and MDM2016-0600 of the Ministerio de Ciencia, Innovación y Universidades, Spain.

Conflicts of Interest: The authors declare no conflict of interest.

References:

1. P. Burke, et al., "Towards a single-chip, implantable RFID system: is a single-cell radio possible?", Biomed Microdevices, 12, 589-596 (2010).
2. D. Ren, et al., "An ultra-high bandwidth nano-electronic interface to the interior of living cells with integrated fluorescence readout of metabolic activity", Scientific Reports, 10, 10756 (2020).
3. P. Abgrall, et al., "Lab-on-chip technologies: making a microfluidic network and coupling it into a complete microsystem - a review", J. Micromech. Microeng., 17, R15–R49 (2007).
4. K. Yang, et al., "Novel developments in mobile sensing based on the integration of microfluidic devices and smartphones", Lab Chip, 16, 943-958 (2016).
5. C. G. Hales, "The origins of the brain's endogenous electromagnetic field and its relationship to provision of consciousness", J. Integr. Neurosci., 13, 313-361 (2014).
6. J. W. Lichtman, et al., "The Big and the Small: Challenges of Imaging the Brain's Circuits", Science, 334, 618 (2018).
7. J. P. Stratford, et al., "Electrically induced bacterial membrane-potential dynamics correspond to cellular proliferation capacity", PNAS, 116, 9552-9557 (2019).
8. A. Ram and A.W. Lo, "Is Smaller Better? A Proposal to Use Bacteria For Neuroscientific Modeling", Front. Comput. Neurosci., 12, 7 (2018).
9. V. Pikov, et al., "Modulation of neuronal activity and plasma membrane properties with low-power millimeter waves in organotypic cortical slices" J. Neural Eng., 7, 045003 (2010).
10. M. N. Shneider, et al., "Initiation and blocking of the action potential in an axon in weak ultrasonic or microwave fields", Phys. Rev. E, 89, 052713 (2014).
11. J. M. Benarroch, et al., "The Microbiologist's Guide to Membrane Potential Dynamics", Trends in Microbiology, 28, 304-314 (2020).
12. P. Fuentes, et al., "ITGB3-mediated uptake of small extracellular vesicles facilitates intercellular communication in breast cancer cells", Nature Com., 11, 4261 (2020).
13. Z. Wan, et al., "Exosome-mediated cell-cell communication in tumor progression", Am. J. Cancer Res., 8, 1661–1673 (2018).
14. M. N. Shneider, et al., "Non-thermal mechanism of weak microwave fields influence on nerve fiber", J. Appl. Phys., 114, 104701 (2013).
15. C. Bot, et al., "Probing the membrane potential of living cells by dielectric spectroscopy", European Biophysics Journal, 38, 1049-1059 (2009).
16. N. Haanbæk, et al., "Development of a Microfluidic GHz Impedance Cytometer", Tech. Messen, 80, 12 (2013).
17. F. Caselli, et al., "Numerical Investigation of a Novel Wiring Scheme Enabling Simple and Accurate Impedance Cytometry", Micromachines, 8, 283 (2017).
18. R. Reale, et al., "Electrical measurement of cross-sectional position of particles flowing through a microchannel", Microfluidics and Nanofluidics, 22, 41 (2018).
19. P. Mehrotra, et al., "EM-Wave Biosensors: A Review of RF, Microwave, mm-Wave and Optical Sensing", Sensors, 19, 1013 (2019).
20. Dau-Chyrh Chang, et al., "Tradeoff study of microwave imaging for biomedical application", IEEE MTT-S Int. Microwave RF Wireless Tech. Biomed. Health. (IMWS-BIO) (2013).
21. J.-C. Bolomey, "Advancing Microwave-Based Imaging Techniques for Medical Applications in the Wake of the 5G Revolution", 13th European Conference on Antennas and Propagation (EuCAP 2019).
22. J. Bao, et al., "Novel Fabrication Process for Integration of Microwave Sensors in Microfluidic Channels", Micromachines, 11, 320 (2020).
23. J. Bao, et al., "A Microwave Platform for Reliable and Instant Interconnecting Combined with Microwave-Microfluidic Interdigital Capacitor Chips for Sensing Applications", Sensors, 20, 1687 (2020).
24. T. Markovic, et al., "An Interdigital Capacitor for Microwave Heating at 25 GHz and Wideband Dielectric Sensing of nL Volumes in Continuous Microfluidics", Sensors, 19, 715 (2019).
25. J. Kilpijärvi, et al., "Microfluidic Microwave Sensor for Detecting Saline in Biological Range", Sensors, 19, 819 (2019).
26. G. Crupi, et al., "Biosensor Using a One-Port Interdigital Capacitor: A Resonance-Based Investigation of the Permittivity Sensitivity for Microfluidic Broadband Bioelectronics Applications", Electronics, 9, 340 (2020).
27. M. Pekker, et al., "Comment on Non-thermal mechanism of weak microwave fields influence on neurons [J. Appl. Phys. 119, 104701 (2013)]," J. Appl. Phys., 119, 086101 (2016).
28. L. Jofre, et al., "Medical Imaging with a Microwave Tomography Scanner", IEEE Trans. Biomedical Eng., 37, 303-312 (1990).
29. N.-T. Nguyen, S.T. Wereley, "Fundamentals and Applications of Microfluidics", Artech House (2006).
30. D. Di Carlo, "Inertial microfluidics", Lab Chip, 9, 3038-3046 (2009).
31. C. Holzner, et al., "Elasto-Inertial Focusing of Mammalian Cells and Bacteria Using Low Molecular, Low Viscosity PEO Solutions", Ana. Chem., 89, 11653-11663 (2017).
32. M. Asghari, et al., "Sheathless Microflow Cytometry Using Viscoelastic Fluids", Scientific Reports, 7, 12342 (2017).
33. Y. Gou, et al., "Progress of Inertial Microfluidics in Principle and Application", Sensors, 18, 1762 (2018).
34. A. Leshansky, et al., "Tunable nonlinear viscoelastic focusing in a microfluidic device", Phys. Rev. Lett., 98, 234501 (2007).
35. A. Leshansky, et al., "Methods for viscoelastic focusing of particles", US8642288, granted patent (priority date 2008).

36. A. H. Raffiee, "Numerical investigation of elasto-inertial particle focusing patterns in viscoelastic microfluidic devices", J. Non-Newtonian Fluid Mech., 272, 104166 (2019).
37. R. B. Brown and J. Audet, "Current techniques for single-cell lysis", Journal of the Royal Society Interface, 5, S131-S138 (2008).
38. L. Nan, et al., "Emerging microfluidic devices for cell-lysis: a review", Lab Chip, 14, 1060 (2014).
39. T. Luo, et al., "Microfluidic Single-Cell Manipulation and Analysis: Methods and Applications", Micromachines, 10, 104 (2019).
40. J. M. Perez, et al., "An image cytometer based on angular spatial frequency processing and its validation for rapid detection and quantification of waterborne microorganisms", Analyst, 140, 7734-7741 (2015).
41. F. Abbasian, et al., "Microbiological Sensing Technologies: A Review", Bioengineering, 5, 20 (2018).
42. S. Vigneshvar, et al., "Recent Advances in Biosensor Technology for Potential Applications - An Overview", Front. Bioeng. Biotech., 4, 11 (2016).
43. A. Vembadi, et al., "Cell Cytometry: Review and Perspective on Biotechnological Advances", Front. Bioeng. Biotechnol., 7, 147 (2019).
44. N. Singhal, et al., "MALDI-TOF mass spectrometry: an emerging technology for microbial identification and diagnosis", Front. Microbio., 6, 791 (2015).
45. R. Franco-Duarte, et al., "Advances in Chemical and Biological Methods to Identify Microorganisms - From Past to Present", Microorganisms, 7, 130 (2019).
46. D. Grieshaber, et al., "Electrochemical biosensors - Sensor Principles and Architectures", Sensors, 8, 1400-1458 (2008).
47. J. Law, et al., "Rapid methods for the detection of foodborne bacterial pathogens: principles, applications, advantages and limitations", Front. Microbio., 5, 770 (2015).
48. G.-B. Lee, et al., "Micro flow cytometers with buried SU-8/SOG optical waveguide", Sensors and Actuators A, 103, 165-170 (2003).
49. S. Etcheverry, et al., "High performance micro-flow cytometer based on optical fibres", Scientific Reports, 7, 5628 (2017).
50. E. M. Goldberg, et al., "Method, system, and compositions for cell counting and analysis", US Pat. 2010/0261197 (2010).
51. B. Li, et al., "Gradient Microfluidics Enables Rapid Bacterial Growth Inhibition Testing", Anal. Chem., 86, 3131-3137 (2014).
52. Y. Matsumoto, et al., "A Microfluidic Channel Method for Rapid Drug-Susceptibility Testing of Pseudomonas aeruginosa", Plos One, 11, e0148797 (2016).
53. F. Hsiung, et al., "Comparison of Count Reproducibility, Accuracy, and Time to Results between a Hemocytometer and the TC20 Automated Cell Counter", Technical Document BioRad, ed BioRad, 1-4 (2013).
54. S. W. Graves, et al., "Nozzle Design Parameters and Their Effects on Rapid Sample Delivery in Flow Cytometry", Cytometry, 47, 127-137 (2002).
55. B. K. McKenna, et al., "A Parallel Microfluidic Flow Cytometer for High Content Screening", Nature Methods, 8, 401-403 (2011).
56. Z. Göröcs, et al., "Giga-pixel fluorescent imaging over an ultra-large field-of-view using a flatbed scanner", Lab Chip, 13, 4460-4466 (2013).
57. R. Narang, et al., "Sensitive, Real-time and Non-Intrusive Detection of Concentration and Growth of Pathogenic Bacteria using Microfluidic-Microwave Ring Resonator Biosensor", Sci. Reports, 8, 15807 (2018).
58. H. Li, et al., "Differentiation of live and heat-killed E. coli by microwave impedance spectroscopy", Sensors and Actuators B, 255, 1614-1622 (2018).
59. N. Jankovic, et al., "A Microwave Microfluidic Sensor Based on a Dual-Mode Resonator for Dual-Sensing Applications", Sensors, 17, 2713 (2017).
60. K. Grenier, et al., "Integrated Broadband Microwave and Microfluidic Sensor Dedicated to Bioengineering", IEEE Trans. Microwave Theory and Techniques, 57, 3246-3253 (2009).
61. J.-C. Chien, et al., "A high-throughput flow cytometry-on-a-CMOS platform for single-cell dielectric spectroscopy at microwave frequencies", Lab Chip, 18, 2065-2076 (2018).
62. G. A. Ferrier, et al., "Microfluidic electromanipulation with capacitive detection for the mechanical analysis of cells", Biomicrofluidics, 2, 044102 (2008).
63. N. Haandbæk, et al., "Resonance-enhanced microfluidic impedance cytometer for detection of single bacteria", Lab Chip, 14, 3313 (2014).
64. L. Yang, et al., "Quantification of Virus Particles Using Nanopore-Based Resistive-Pulse Sensing Techniques", Front. Microbio., 7, 1500 (2016).
65. D. Holmes, et al., "Single Cell Impedance Cytometry for Identification and Counting of CD4 T-Cells in Human Blood Using Impedance Labels", Anal. Chem., 82, 1455-1461 (2010).
66. A. Pandey, et al., "Graphene-interfaced electrical biosensor for label-free and sensitive detection of foodborne pathogenic E. coli O157:H7", Biosensors and Bioelectronics, 91, 225-231 (2017).
67. K. Cheung, et al., "Microfluidic impedance spectroscopy flow cytometer: particle size calibration", Proceedings of the IEEE International Conference on Micro Electro Mechanical Systems (MEMS) (2004).
68. D. Spencer, et al., "High-Speed Single-Cell Dielectric Spectroscopy", ACS Sens, 5, 423-430 (2020).
69. D. R. Hristov, et al., "Designing Paper-Based Immunoassays for Biomedical Applications", Sensors, 19, 554 (2019).
70. I. Sinn, et al., "Asynchronous magnetic bead rotation (AMBR) biosensor in microfluidic droplets for rapid bacteria growth and susceptibility measurements", Lab Chip, 11, 2604 (2011).
71. C. Petchakup, et al., "Advances in Single Cell Impedance Cytometry for Biomedical Applications", Micromachines, 8, 87 (2017).

72. L. Byerly, et al., “Machine for rapidly counting and measuring the size of small nematodes”, Review of Scientific Instruments, 46, 517 (1975).
73. R. A. Hoffman, et al., “Flow cytometric electronic direct current volume and radiofrequency impedance measurements of single cells and particles” Cytometry, 1, 377–384 (1981).
74. J. M. Martel and M. Toner, “Inertial focusing in microfluidics”, Annual Review of Biomedical Engineering, 16, 371-396 (2014).
75. F. M. White, “Fluid Mechanics”, McGraw-Hill (2016).
76. G. Segré, et al., “Radial particle displacements in Poiseuille flow of suspensions”, Nature, 189, 209-210 (1961).
77. D. Di Carlo, et al., "Continuous inertial focusing, ordering, and separation of particles in microchannels", PNAS USA, 104, 18892-97 (2007).
78. A. Karnis, et al., “Particle motions in sheared suspensions. XIX. Viscoelastic media”, Transactions of the Society of Rheology, 10, 571-592, (1966).
79. B. P. Ho, et al., “Migration of rigid spheres in a two-dimensional unidirectional shear flow of a second-order fluid”, J. Fluid Mech., 65, 365-400 (1976).
80. R. G. Cox, et al., “The lateral migration of solid particles in a laminar flow near a plane”, International Journal of Multiphase Flow, 3, 201-222 (1977).
81. B. R. Mutlu, et al., "Oscillatory inertial focusing in infinite microchannels", PNAS USA, 115, 7682-7687 (2018).
82. J. Matas, et al., “Trains of particles in finite-Reynolds-number pipe flows”, Physics of Fluids, 16, 4192-4195 (2004).
83. S. Yang, et al., "Sheathless elasto-inertial particle focusing and continuous separation in a straight rectangular microchannel", Lab Chip, 11, 266-273 (2010).
84. J. R. Womersley, “Method for the calculation of velocity, rate of flow and viscous drag in arteries when the pressure gradient is known”, J. Physiol., 127, 553-563 (1955).
85. K. Asami, et al., “Dielectric Approach to Suspensions of Ellipsoidal Particles Covered with a Shell in Particular Reference to Biological Cells”, Jpn. J. Appl. Phys., 19, 359 (1980).
86. S.-S. Tuca, et al., “Calibrated complex impedance of CHO cells and E. coli bacteria at GHz frequencies using scanning microwave microscopy”, Nanotechnology, 27, 135702 (2016).
87. W. C. Chew, “Waves and fields in inhomogeneous media”, Wiley-IEEE Press, 9780470547052 (1995).
88. C. Balanis, “Advanced Engineering Electromagnetics”, Wiley, 978-0-470-58948-9 (2012).
89. A. Ishimaru, “Electromagnetic wave propagation, radiation, and scattering from fundamentals to applications”, Wiley-IEEE Press, 978-1-118-09881-3 (2017).
90. A. Wolski, “Theory of Electromagnetic Fields”, CERN Accelerator School CAS 2010 (2011).
91. “C95.1-1991 - IEEE Standard for Safety Levels with Respect to Human Exposure to Radio Frequency Electromagnetic Fields, 3 kHz to 300 GHz”, IEEE C95.1-1991 (1997).
92. G. Franceschetti, “Electromagnetic Biointeraction: Mechanisms, Safety Standards, Protection Guides ”, Springer, (1989).
93. M. Zhadobov, et al., “Numerical and experimental millimeter-wave dosimetry for in vitro experiments”, IEEE Trans. Microwave. Theory Tech., 56, 2998–3007 (2008).
94. J. Platkiewicz and R. Brette, “A threshold equation for action potential initiation”, PLoS Comput. Biol., 6, e1000850 (2010).
95. M. N. Shneider, et al., “Interaction between electrolyte ions and the surface of a cell lipid membrane”, J. Phys. Chem. Biophys., 5, 177 (2015).
96. Y. L. Drean, et al., “State of knowledge on biological effects at 40–60 GHz”, C. R. Phys., 14, 402–411 (2013).
97. A. V. Vorst, et al., “RF/Microwave Interaction with Biological Tissues”, John Wiley & Sons, Inc. (2006).
98. A. Garrido, “Electromagnetic Characterization of Living Microorganisms”, PhD thesis dissertation, Technical University of Catalonia - UPC (2018). https://upcommons.upc.edu/handle/2117/117762
99. F. Zarrinkhat, A. Garrido, L. Jofre, et al., “Electromagnetic Monitoring of Biological Microorganisms”, 13th European Conference on Antennas and Propagation (EuCAP 2019).
100. H. Lodish, et al., “Molecular Cell Biology, 4th edition”, W. H. Freeman (2000).
101. F. S. Barnes, at al., “Bioengineering and Biophysical Aspects of Electromagnetic Fields”, Taylor & Francis Group (2006).
102. R. Lescanne, et al., “Irreversible Qubit-Photon Coupling for the Detection of Itinerant Microwave Photons”, Phys. Rev. X, 10, 021038 (2020).
103. X. Zhang, et al., “High-Sensitivity Microwave Sensor for Liquid Characterization Using a Complementary Circular Spiral Resonator”, Sensors, 19, 787 (2019).
104. A. A. Abduljabar, et al., “Modelling and Measurements of the Microwave Dielectric Properties of Microspheres”, IEEE Trans. Microwave Theor. and Techniques, 62, 4492-4500 (2015).
105. W.F. Pickard, ”Does the resting potential of Chara Braumi have an electrogenic component?”, Can. J. Bol., 51, 715 (1973).
106. G. Franceschetti, “Cell Membrane Nonlinear Response to an Applied Electromagnetic Field”, IEEE Trans. Microwave Theor. and Techniques, 32, 653-658 (1984).
107. A.L. Hodgkin, et al., “A quantitative description of membrane current and its application to conduction and excitation in nerve”, J. Physiol., 117, 500-544 (1952).
108. R. Fitzhugh, “Impulses and physiological states in theoretical models of nerve membrane”, J. Biophys., 1, 445-466 (1961).
109. E. M. Izhikevich, “Simple model of spiking neurons”, IEEE Trans. Neural Networks, 14, 1569-1572 (2003).
110. P. E. Phillipson, et al., “A Comparative Study of the Hodgkin-Huxley and Fitzhugh-Nagumo Models of Neuron Pulse Propagation”, Int. J. Bifurcation and Chaos, 15, 3851-3866 (2005).

111. L. N. Miller, et al., "Second Harmonic Generation Spectroscopy of Membrane Probe Dynamics in Gram-Positive Bacteria", Biophysical Journal, 117, 1419-1428 (2019).
112. B. A. Nemet, et al., "Second harmonic imaging of membrane potential of neurons with retinal", J. Biomedical Optics, 9, 873-881 (2004).
113. S. Gambhir, et al. "Intrinsic Nonlinearity of a PN-junction Diode and Higher Order Harmonic Generation", Physics Education, 34, 2 (2018).
114. F. Steinlechner, et al., "Efficient heralding of polarization-entangled photons from type-0 and type-II spontaneous parametric downconversion in periodically poled KTiOPO4", J. OSA B, 31, 2068-2076 (2014).
115. K. Chang, "Encyclopedia of RF and Microwave Engineering, 6 Volume", Wiley (2005).
116. T. May, et al., "Design, realization, and characteristics of a transition edge bolometer for sub-millimeter wave astronomy," Review of Scientific Instruments, 83, 114502 (2012).
117. S. Barzanjeh, et al., "Microwave quantum illumination using a digital receiver", Science Advances, 6, eabb0451 (2020).